

Trajectory optimization for a class of robots belonging to Constrained Collaborative Mobile Agents (CCMA) family

Nitish Kumar*, Stelian Coros

Abstract—We present a novel class of robots belonging to Constrained Collaborative Mobile Agents (CCMA) family which consists of ground mobile bases with non-holonomic constraints. Moreover, these mobile robots are constrained by closed-loop kinematic chains consisting of revolute joints which can be either passive or actuated. We also describe a novel trajectory optimization method which is general with respect to number of mobile robots, topology of the closed-loop kinematic chains and placement of the actuators at the revolute joints. We also extend the standalone trajectory optimization method to optimize concurrently the design parameters and the control policy. We describe various CCMA system examples, in simulation, differing in design, topology, number of mobile robots and actuation space. The simulation results for standalone trajectory optimization with fixed design parameters is presented for CCMA system examples. We also show how this method can be used for tasks other than end-effector positioning such as internal collision avoidance and external obstacle avoidance. The concurrent design and control policy optimization is demonstrated, in simulations, to increase the CCMA system workspace and manipulation capabilities. Finally, the trajectory optimization method is validated in experiments through two 4-DOF prototypes consisting of 3 tracked mobile bases.

Index Terms—Parallel Robots, Optimization and Optimal Control, Multi-Robot Systems

I. INTRODUCTION

A. Motivation

Mechanisms are fundamental to address problems of robotic manipulation involving motion generation and force transmission. Examples include serial mechanisms such as industrial manipulators and closed-loop kinematic mechanisms such as pick and place delta robots or cable driven robots. Different types of mobile platforms such as aerial quadcopters, ground mobile robots (omni-directional, tracked, wheeled) and legged robots provide solutions to the problem of robotic mobility. Several important applications such as field robotics, construction robotics [1], [2], [3], [4], [5], service robotics require robots to be mobile as well as able to do manipulation tasks. Interfacing a single mobile base with a serial manipulator [6], [7] or multiple mobile bases with closed-loop kinematic chains [8] is a potential solution to solving both the challenges of global mobility and local manipulation. Instead of idealizing such systems as monolithic robots designed once in its lifetime for a particular task, our long term goal is to investigate them within a much broader abstraction of heterogeneous,

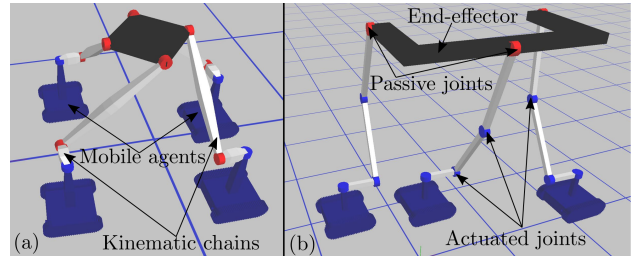


Fig. 1: Constrained collaborative mobile agents concept: a number of mobile bases $0, 1 \dots n_m - 1$ constrained with active-passive closed-loop kinematic chains (gray bars connected with red passive joints and blue actuated joints) manipulating an end-effector (black polygon).

modular, mobile, multi-robot and reconfigurable systems. Our vision is a ubiquitous robot ecosystem which is highly mobile, modular, customizable with heterogeneous components and readily operational for varied tasks.

The idea of interfacing multiple mobile bases with closed-loop kinematic chains presents a huge potential to exploit the large design space for task-based customization and reconfiguration of modular mobile multi-robot systems. Moreover, if a subset of joints in the closed-loop kinematic chains are actuated, a large control space can be generated for active-passive closed-loop kinematic chains. This could especially be useful in optimizing the stiffness or payload capacity of the system. In our previous work [8], we introduced the concept of Constrained Collaborative Mobile Agents (CCMA). In this paper, we are continuing this work and introduce another novel class of robots belonging to CCMA family (Fig. 1), which has non-holonomic bases and active-passive closed-loop kinematic chains with revolute joints.

The focus of this paper is on the motion generation capabilities of the CCMA systems. In this respect, one of the most important tasks of a mobile robotic system is the gross manipulation or gross positioning of a more precise robotic end-effector. For mobile bases with non-holonomic constraints, this task is non-trivial and requires trajectory optimization techniques. Moreover, the closed-loop kinematic chains along with the actuation of a subset of joints impose even more kinematic constraints on the motion of the mobile agents. Therefore, we develop and present a novel framework for kinematic motion planning and trajectory optimization for the class of the robots presented in this paper. We also extend this trajectory optimization method to allow design optimization concurrently.

Nitish Kumar and Stelian Coros are with the Computational Robotics Lab in the Institute for Intelligent Interactive Systems (IIS), ETH Zurich Switzerland. {nitish.kumar@inf.ethz.ch, stelian.coros@inf.ethz.ch}

* corresponding author

B. Related work

An architectural scale installation was built through collaboration between multiple aerial quadcopters in the work [9]. A mobile cable driven system using multiple mobile bases was demonstrated in the work [10], [11] for logistics applications. Mobile parallel robots with multiple omnidirectional mobile bases was presented in the work [12], [13], [14]. In this paper, we present a novel class of multi-robot collaborative systems, which has multiple non-holonomic wheeled mobile bases constrained with active-passive closed-loop kinematics chains.

Interesting examples of mobile robotic systems with fully actuated legs, and wheels with non-holonomic constraints have been proposed in the work [15], [16], [17]. In the current work, the closed-loop kinematic chains in the CCMA system examples need not be fully actuated. Therefore, the class of robots introduced in the paper exhibit a vast design and actuation space with fully passive to fully actuated revolute joints.

An overview of planning methods for robotic systems with non-holonomic constraints can be found in the work [18], [19], [20]. The trajectory optimization and kinematic motion planning method presented in the current paper complements other optimal control approaches [15], [16], [21], [17] and sampling based approaches [22], [23], [24]. However none of these optimal control or sampling based approaches for trajectory optimization or motion planning discuss the possibility to do concurrent design and control policy optimization over a trajectory. In our approach, the design parameters of the mobile multi-robot system can be optimized and updated along with control policy during the trajectory optimization step. This could specially be powerful when the process or task itself is evolving during initial conception stages and could require several design iterations of a modular, mobile, multi-robot system. In our method, rigid body kinematics is modeled on a constraint based formulation presented in the paper [25], [26]. For our trajectory optimization technique, we calculate the derivatives of the kinematic constraints analytically, required for the gradient-based methods (e.g. L-BFGS, Gauss-Newton), using sensitivity analysis techniques [27], [28], [29], [30], [31], [32].

C. Contributions

In this paper, contributions are two-fold. First contribution is the development of a novel hardware architecture consisting of multiple mobile agents, with non-holonomic constraints, further constrained by active-passive closed-loop kinematic chains manipulating an end-effector. We present, in simulation, several designs ranging in design parameters, degrees of freedom (DOF), morphology, number of mobile agents and number of actuated joints showing the potential for scalability, task-adaptability and reconfigurability.

The second contribution is the development of the optimization framework for concurrent design and trajectory optimization, and kinematic motion planning of the CCMA system. Our optimization framework is independent of design parameters, DOF, morphology, number of mobile agents

and number of actuated joints in a CCMA system. We further evaluate this optimization framework on several CCMA system examples and demonstrate several tasks ranging from gross end-effector positioning, internal mobile agents collision avoidance to external obstacle collision avoidance.

II. CONSTRAINED COLLABORATIVE MOBILE AGENTS SYSTEM - DESCRIPTION AND MODELING

The Fig. 1 illustrates an instantiation of the CCMA concept presented in this paper. It consists of active-passive closed-loop kinematic chains connecting the end-effector to a number of mobile bases with non-holonomic constraints. The mobile agents along with a set of actuated joints in the closed-loop kinematic chains, form the actuators in the system to control the end-effector. The mobile agents (wheeled or tracked systems with non-holonomic constraints) have 2-DOF each. Fig. 1(a) shows a system example with 4 mobile bases and active kinematic chains consisting of one actuated joint each. Fig. 1(b) shows a system example with 3 mobile bases and active kinematic chains consisting of three actuated joints each.

A. Notations and preliminaries

n_b	total number of rigid bodies in CCMA system.
n_m	number of mobile robots.
n_a	number of actuated joints.
n_t	number of states in the trajectory.
\mathbf{st}_j	intermediate state vector of the system at time t_j which has a size of $6 \cdot n_b$, where $j = 0, 1, 2, \dots, n_t$.
\mathbf{u}_j	intermediate control vector which takes the state \mathbf{s}_j to \mathbf{s}_{j+1} in time step δt . The size of \mathbf{u}_j is $2 \cdot n_m + n_a$. It is formed by stacking the linear and angular speed of all mobile bases followed by angular speed of all actuated rotary joints.
\mathbf{a}_j	it is formed by stacking the x, y components of the linear velocity and, angular speed of the mobile bases followed by angular speeds of the actuated rotary joints. The size of \mathbf{a}_j is $3 \cdot n_m + n_a$.
\mathbf{m}_j	it contains the absolute values of the mobile base poses and rotary actuator angles. Specifying this vector also specifies the state \mathbf{s}_j of CCMA system. The size of \mathbf{m}_j is $3 \cdot n_m + n_a$.
\mathbf{dp}	vector of design parameters. In this paper, we consider the kinematic parameters, affecting geometry of the rigid bodies, which have impact on the motion generation capability and workspace.
\mathbf{C}_j	a vector of constraints, corresponding to state \mathbf{st}_j , which include the constraints output by (a) each passive joint (b) kinematic constraints which correspond to the planar constraint on the mobile robot (c) mobile robot actuator constraints assuming two motorized prismatic actuators along \mathbf{x}_g , \mathbf{y}_g and a rotary actuator along \mathbf{z}_g . (\mathbf{O}_g , \mathbf{x}_g , \mathbf{y}_g , \mathbf{z}_g) represent world reference frame with origin at \mathbf{O}_g and three unit vectors along \mathbf{x}_g , \mathbf{y}_g , \mathbf{z}_g d) each rotary actuator which are obtained by fixing the value of angle in the motorized joint. The mathematical modeling

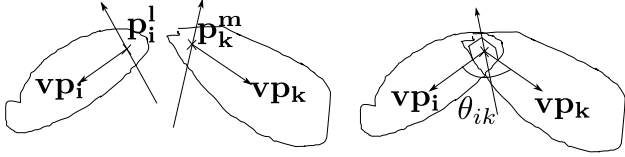


Fig. 2: Two rigid bodies i and k connected by a revolute joint connection and a rotary actuator fixing the value of θ_{ik} .

of the constraints for (a), (b) and (c) is described in our previous paper [8].

\mathbf{st} , \mathbf{u} , \mathbf{a} and \mathbf{m} are trajectory vectors obtained after stacking the vectors \mathbf{st}_j , \mathbf{u}_j , \mathbf{a}_j and \mathbf{m}_j , respectively.

1) Rotary actuator constraints between two rigid bodies:

A rigid body i has 6-DOF which is described by its state $\mathbf{s}_i = [\gamma_i, \beta_i, \alpha_i, \mathbf{T}_i]$. \mathbf{s}_i consists of three Euler angles and translation vector $\mathbf{T}_i = [x_i, y_i, z_i]$ from global reference frame to rigid body local co-ordinate system. Thus any point $\bar{\mathbf{p}}_i$ or free vector $\bar{\mathbf{v}}_i$ expressed in local co-ordinate system of a rigid body i can be converted to global world co-ordinates as $\mathbf{p}_i = \mathbf{R}_{\gamma_i} \cdot \mathbf{R}_{\beta_i} \cdot \mathbf{R}_{\alpha_i} \cdot \bar{\mathbf{p}}_i + \mathbf{T}_i$ or $\mathbf{v}_i = \mathbf{R}_{\gamma_i} \cdot \mathbf{R}_{\beta_i} \cdot \mathbf{R}_{\alpha_i} \cdot \bar{\mathbf{v}}_i$. \mathbf{R} is an elementary 3×3 rotation matrix.

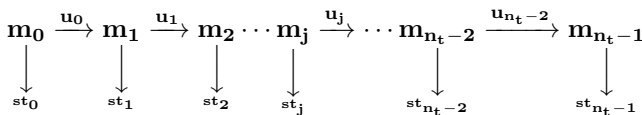
Let $\bar{\mathbf{v}}_{\mathbf{p}_i}$ and $\bar{\mathbf{v}}_{\mathbf{p}_k}$ be two unit vectors in the plane perpendicular to the rotation axis and attached to rigid body i and k at points $\bar{\mathbf{p}}_i^l$ and $\bar{\mathbf{p}}_k^m$ (Fig. 2), respectively. Let θ_{ik} be angle between $\bar{\mathbf{v}}_{\mathbf{p}_i}$ and $\bar{\mathbf{v}}_{\mathbf{p}_k}$ about the common rotation axis. Fixing the angle of rotary actuator by θ_{ik} imposes the constraint $\mathbf{C}_{ik}^a = [\mathbf{R}_{\gamma_i} \cdot \mathbf{R}_{\beta_i} \cdot \mathbf{R}_{\alpha_i} \cdot (\mathbf{R}_{\theta_{ik}} \cdot \bar{\mathbf{v}}_{\mathbf{p}_i}) - \mathbf{R}_{\gamma_k} \cdot \mathbf{R}_{\beta_k} \cdot \mathbf{R}_{\alpha_k} \cdot \bar{\mathbf{v}}_{\mathbf{p}_k}]$.

2) Design parameters \mathbf{dp} : Each rigid body i geometry is defined by a number of points, such as the l^{th} point $\bar{\mathbf{p}}_i^l$ on it (Fig. 2). Let $\bar{\mathbf{p}}_i^l = \bar{\mathbf{p}}_i^l$ before the start of the design optimization. A design parameter dp_i^l is defined to modify every such point on the rigid body as follows: $\bar{\mathbf{p}}_i^l = \bar{\mathbf{p}}_i^l + dp_i^l \cdot \frac{\bar{\mathbf{p}}_i^l}{\|\bar{\mathbf{p}}_i^l\|}$. The continuous scalar variable dp_i^l can take both positive and negative values. Therefore, \mathbf{dp} accumulates these design parameters for every defined point on each rigid body in the CCMA system. These parameters can implicitly define the length of a link or geometry of a polygonal end-effector or support polygon of a mobile base, in a CCMA system.

III. OPTIMIZATION FRAMEWORK

A. Forward simulation of the system state trajectory \mathbf{st} for given control input \mathbf{u} and design parameters \mathbf{dp}

Following schematic shows the system state trajectory evolution, when control inputs $\mathbf{u}_j, j = 0, 1, 2, 3 \dots n_t - 2$ is successively applied starting from state \mathbf{st}_0 .



In order to calculate the next state \mathbf{st}_{j+1} from a starting state \mathbf{st}_j and control input \mathbf{u}_j , we solve an optimization

problem and minimize an energy E_j which is sum of the mechanism constraint violations as below:

$$\mathbf{st}_{j+1} = \arg \min_{\mathbf{st}} [E_j(\mathbf{m}_j, \mathbf{st}, \mathbf{u}_j, \mathbf{dp}) = \frac{1}{2} \mathbf{C}_j^T \mathbf{C}_j] \quad (1)$$

For mobile base $k = 0, 1, 2 \dots (n_m - 1)$ with non-holonomic constraints:

$$\begin{aligned} \mathbf{u}_j[2k] &= \text{linear velocity of the mobile robot } k \text{ in state } \mathbf{st}_j \\ \mathbf{u}_j[2k+1] &= \text{angular velocity of the mobile robot } k \text{ in } \mathbf{st}_j \\ \mathbf{a}_j[3k+1] &= \text{component of the linear velocity along } \mathbf{x}_g \\ \mathbf{a}_j[3k+2] &= \text{component of the linear velocity along } \mathbf{y}_g \\ \theta_{j,k}^m &= \mathbf{m}_j[3k] = \text{global orientation of the mobile robot} \\ \mathbf{a}_j[3k] &= \mathbf{u}_j[2k]; \quad \mathbf{a}_j[3k+1] = \mathbf{u}_j[2k+1] \cdot \cos(\theta_{j,k}^m) \\ \mathbf{a}_j[3k+2] &= \mathbf{u}_j[2k+1] \cdot \sin(\theta_{j,k}^m) \\ \mathbf{a}_j &= f_j(\mathbf{u}_j, \mathbf{m}_j) \end{aligned} \quad (2)$$

Eqn. 2 implicitly takes into account the non-holonomic constraints while updating \mathbf{a}_j from the \mathbf{u}_j and \mathbf{m}_j . Therefore, the non-holonomic constraints are always satisfied within the forward simulation step itself. They are never optimized as part of the trajectory optimization step which is described in the next subsection.

The state transition Eqn. 1 can also be written as a function of \mathbf{m}_{j+1} as below:

$$\begin{aligned} \mathbf{m}_{j+1} &= \mathbf{m}_j + f_j(\mathbf{u}_j, \mathbf{m}_j) \cdot \delta t \\ \mathbf{st}_{j+1} &= \arg \min_{\mathbf{st}} E_j(\mathbf{m}_{j+1}, \mathbf{st}, \mathbf{dp}) \end{aligned} \quad (3)$$

B. Trajectory optimization leading to calculation of the control input evolution \mathbf{u} and design parameters \mathbf{dp}

We solve an optimization problem where an objective function \mathcal{O} is evaluated over the entire trajectory, and minimized to calculate the control inputs $\mathbf{u}_0, \mathbf{u}_1 \dots \mathbf{u}_j \dots \mathbf{u}_{n_t-2}$ and design parameters \mathbf{dp} . The design parameters \mathbf{dp} remain the same when successive control inputs $\mathbf{u}_0, \mathbf{u}_1 \dots \mathbf{u}_j \dots \mathbf{u}_{n_t-2}$ are applied and they are updated along with \mathbf{u} at start of each optimization step.

The assumption of the sensitivity analysis (Sec. III-B.1) states that as result of the optimization upon convergence, in Eqn. 3, we get gradient of energy function E_j , $\mathbf{g}_j(\mathbf{m}_j, \mathbf{st}_{j+1}, \mathbf{u}_j, \mathbf{dp}) = 0$ for all \mathbf{u}_j and \mathbf{dp} . This does not ensure, however, that the residual constraint energy $E_{rj} = E_j(\mathbf{m}_{j+1}, \mathbf{st}_{j+1}, \mathbf{dp})$ after optimization, from the forward simulation step, will be zero. Therefore, we add the residual constraint energies to the objective function \mathcal{O} to make sure that the remaining residual constraint energies also go to zero during the trajectory optimization.

$$\begin{aligned} \arg \min_{\mathbf{u}, \mathbf{dp}} \quad \mathcal{O}(\mathbf{st}, \mathbf{u}, \mathbf{m}, \mathbf{dp}) &= \\ & \sum_{i=0}^{n_{task}-1} w_i \cdot \mathcal{O}_{task_i}(\mathbf{st}, \mathbf{u}, \mathbf{m}, \mathbf{dp}) + \\ & \lambda_E \cdot \sum_{j=0}^{n_t-1} E_j(\mathbf{m}_{j+1}, \mathbf{st}_{j+1}, \mathbf{dp}) \end{aligned} \quad (4)$$

In order to solve this optimization problem through a gradient based minimization approach, we need calculation of the gradients of the objection function $\frac{d\mathcal{O}}{d\mathbf{u}_i}$, $i = 0, 1, 2, 3 \dots n_t - 2$ and $\frac{d\mathcal{O}}{d\mathbf{dp}}$, as described in Eqn 5. The parameters \mathbf{m} and \mathbf{dp} are independent of each other.

$$\begin{aligned} \frac{d\mathcal{O}}{d\mathbf{u}_i} &= \frac{\partial \mathcal{O}}{\partial \mathbf{u}_i} + \sum_{j=0}^{n_t-1} \frac{\partial \mathcal{O}}{\partial \mathbf{st}_j} \cdot \frac{d\mathbf{st}_j}{d\mathbf{u}_i} + \sum_{j=0}^{n_t-1} \frac{\partial \mathcal{O}}{\partial \mathbf{m}_j} \cdot \frac{d\mathbf{m}_j}{d\mathbf{u}_i} \\ \frac{d\mathcal{O}}{d\mathbf{dp}} &= \frac{\partial \mathcal{O}}{\partial \mathbf{dp}} + \sum_{j=0}^{n_t-1} \frac{\partial \mathcal{O}}{\partial \mathbf{st}_j} \cdot \frac{d\mathbf{st}_j}{d\mathbf{dp}} \end{aligned} \quad (5)$$

However, calculation of the sensitivities $\frac{d\mathbf{st}_j}{d\mathbf{u}_i}$, $\frac{d\mathbf{m}_j}{d\mathbf{u}_i}$ and $\frac{d\mathbf{st}_j}{d\mathbf{dp}}$ is not possible directly in closed form and is computationally prohibitive using finite differences. Therefore, we make use of the sensitivity analysis to indirectly calculate them analytically.

1) *Sensitivity analysis*: Since control vector \mathbf{u}_k , $k = 0, 1, 2 \dots n_t - 2$ only affects the future states from \mathbf{st}_{k+1} onwards, we can state that $\frac{d\mathbf{st}_j}{d\mathbf{u}_k} = 0$; $\frac{d\mathbf{m}_j}{d\mathbf{u}_k} = 0 \quad \forall j \leq k$. As result of the optimization upon convergence, in Eqn. 1, we get gradient of energy function E_j , $\mathbf{g}_j(\mathbf{m}_j, \mathbf{st}_{j+1}, \mathbf{u}_j, \mathbf{dp}) = 0$ for all \mathbf{u}_j . The parameters \mathbf{u} and \mathbf{dp} are independent of each other.

$$\begin{aligned} \frac{\partial \mathbf{g}_j}{\partial \mathbf{u}_j} + \frac{\partial \mathbf{g}_j}{\partial \mathbf{m}_j} \cdot \frac{d\mathbf{m}_j}{d\mathbf{u}_j} + \frac{\partial \mathbf{g}_j}{\partial \mathbf{st}_{j+1}} \cdot \frac{d\mathbf{st}_{j+1}}{d\mathbf{u}_j} &= 0 \implies \\ \frac{\partial \mathbf{g}_j}{\partial \mathbf{u}_j} + \frac{\partial \mathbf{g}_j}{\partial \mathbf{st}_{j+1}} \cdot \frac{d\mathbf{st}_{j+1}}{d\mathbf{u}_j} &= 0 \implies \\ \frac{d\mathbf{st}_{j+1}}{d\mathbf{u}_j} &= - \left(\frac{\partial \mathbf{g}_j}{\partial \mathbf{st}_{j+1}} \right)^{-1} \cdot \frac{\partial \mathbf{g}_j}{\partial \mathbf{u}_j} \\ \frac{d\mathbf{st}_{j+1}}{d\mathbf{u}_j} &= \frac{\partial \mathbf{st}_{j+1}}{\partial \mathbf{u}_j} + \frac{\partial \mathbf{st}_{j+1}}{\partial \mathbf{m}_j} \cdot \frac{d\mathbf{m}_j}{d\mathbf{u}_j} = \frac{\partial \mathbf{st}_{j+1}}{\partial \mathbf{u}_j} \\ \frac{d\mathbf{st}_{j+1}}{d\mathbf{u}_j} &= \frac{\partial \mathbf{st}_{j+1}}{\partial \mathbf{a}_j} \cdot \frac{\partial \mathbf{a}_j}{\partial \mathbf{u}_j} \\ \text{it can be shown, } \frac{\partial \mathbf{st}_{j+1}}{\partial \mathbf{a}_j} &= - \left(\frac{\partial \mathbf{g}_j}{\partial \mathbf{st}_{j+1}} \right)^{-1} \cdot \frac{\partial \mathbf{g}_j}{\partial \mathbf{a}_j} \end{aligned}$$

Similarly, gradient of energy function E_j , $\mathbf{g}_j(\mathbf{m}_j, \mathbf{st}_{j+1}, \mathbf{u}_j, \mathbf{dp}) = 0$ for all \mathbf{dp} .

$$\begin{aligned} \frac{\partial \mathbf{g}_j}{\partial \mathbf{dp}} + \frac{\partial \mathbf{g}_j}{\partial \mathbf{m}_j} \cdot \frac{d\mathbf{m}_j}{d\mathbf{dp}} + \frac{\partial \mathbf{g}_j}{\partial \mathbf{st}_{j+1}} \cdot \frac{d\mathbf{st}_{j+1}}{d\mathbf{dp}} &= 0 \implies \\ \frac{\partial \mathbf{g}_j}{\partial \mathbf{dp}} + \frac{\partial \mathbf{g}_j}{\partial \mathbf{st}_{j+1}} \cdot \frac{d\mathbf{st}_{j+1}}{d\mathbf{dp}} &= 0 \implies \\ \frac{d\mathbf{st}_{j+1}}{d\mathbf{dp}} &= - \left(\frac{\partial \mathbf{g}_j}{\partial \mathbf{st}_{j+1}} \right)^{-1} \cdot \frac{\partial \mathbf{g}_j}{\partial \mathbf{dp}} \end{aligned}$$

$\frac{\partial \mathbf{g}_j}{\partial \mathbf{st}_{j+1}}$ is the hessian of the energy E_j evaluated at \mathbf{st}_{j+1} . $\frac{\partial \mathbf{g}_j}{\partial \mathbf{a}_j}$, $\frac{\partial \mathbf{g}_j}{\partial \mathbf{u}_j}$ and $\frac{\partial \mathbf{g}_j}{\partial \mathbf{dp}}$ is how the gradient of the energy E_j changes with change in the input \mathbf{a}_j , \mathbf{u}_j , \mathbf{dp} only, respectively. These terms are calculated analytically. First all sensitivities $\frac{d\mathbf{st}_{j+1}}{d\mathbf{u}_j}$, $j = 0, 1, 2, 3 \dots n_t - 2$ are calculated.

2) *Recurrence relation*: To calculate rest of the sensitivities $\frac{d\mathbf{st}_j}{d\mathbf{u}_k}$, $\frac{d\mathbf{m}_j}{d\mathbf{u}_k}$ for $k+1 < j \leq n_t - 1$; $k = 0, 1, 2, \dots n_t - 2$, we derive and present the following recurrence relation:

$$\begin{aligned} \frac{\partial \mathbf{m}_{j+1}}{\partial \mathbf{a}_j} &= \mathbf{I} \cdot \delta t \quad \text{from Eqn. 3} \\ \frac{\partial \mathbf{st}_{j+1}}{\partial \mathbf{m}_{j+1}} \cdot \delta t &= \frac{\partial \mathbf{st}_{j+1}}{\partial \mathbf{m}_{j+1}} \cdot \frac{\partial \mathbf{m}_{j+1}}{\partial \mathbf{a}_j} = \frac{\partial \mathbf{st}_{j+1}}{\partial \mathbf{a}_j} \\ \frac{\partial \mathbf{st}_{j+1}}{\partial \mathbf{u}_k} &= 0 \quad \forall \quad k \neq j \\ \frac{d\mathbf{st}_{j+1}}{d\mathbf{u}_k} &= \frac{\partial \mathbf{st}_{j+1}}{\partial \mathbf{u}_k} + \frac{\partial \mathbf{st}_{j+1}}{\partial \mathbf{m}_{j+1}} \cdot \frac{d\mathbf{m}_{j+1}}{d\mathbf{u}_k} \\ \frac{d\mathbf{st}_{j+1}}{d\mathbf{u}_k} &= \frac{\partial \mathbf{st}_{j+1}}{\partial \mathbf{a}_j} \cdot \frac{d\mathbf{m}_{j+1}}{d\mathbf{u}_k} \cdot \frac{1}{\delta t} \\ \frac{d\mathbf{m}_{j+1}}{d\mathbf{u}_k} &= \left(\mathbf{I} + \frac{\partial \mathbf{a}_j}{\partial \mathbf{m}_j} \right) \cdot \frac{d\mathbf{m}_j}{d\mathbf{u}_k} \end{aligned} \quad (6)$$

Finally gradients $\frac{d\mathcal{O}}{d\mathbf{u}_i}$, $i = 1, 2, 3 \dots n_t - 1$ and $\frac{d\mathcal{O}}{d\mathbf{dp}}$ can be calculated by substituting the sensitivities $\frac{d\mathbf{st}_j}{d\mathbf{u}_i}$, $\frac{d\mathbf{m}_j}{d\mathbf{u}_i}$ and $\frac{d\mathbf{st}_j}{d\mathbf{dp}}$ in the Eqn. 5.

3) *Residual constraint energies*: The corresponding gradient of the residual constraint energy $E_{rj} = E_j(\mathbf{m}_{j+1}, \mathbf{st}_{j+1}, \mathbf{dp})$ is needed in order to calculate the gradient in the Eqn. 5.

$$\begin{aligned} \frac{\partial E_{rj}}{\partial \mathbf{u}_i} &= 0; \quad \frac{\partial E_{rj}}{\partial \mathbf{st}_{j+1}} = 0 \quad \text{upon convergence in Eqn. 3;} \\ \frac{dE_{rj}}{d\mathbf{u}_i} &= \frac{\partial E_{rj}}{\partial \mathbf{u}_i} + \frac{\partial E_{rj}}{\partial \mathbf{m}_{j+1}} \cdot \frac{d\mathbf{m}_{j+1}}{d\mathbf{u}_i} + \frac{\partial E_{rj}}{\partial \mathbf{st}_{j+1}} \cdot \frac{d\mathbf{st}_{j+1}}{d\mathbf{u}_i} \\ \frac{dE_{rj}}{d\mathbf{u}_i} &= \frac{\partial E_{rj}}{\partial \mathbf{m}_{j+1}} \cdot \frac{d\mathbf{m}_{j+1}}{d\mathbf{u}_i} \\ \frac{dE_{rj}}{d\mathbf{dp}} &= \frac{\partial E_{rj}}{\partial \mathbf{dp}} + \frac{\partial E_{rj}}{\partial \mathbf{m}_{j+1}} \cdot \frac{d\mathbf{m}_{j+1}}{d\mathbf{dp}} + \frac{\partial E_{rj}}{\partial \mathbf{st}_{j+1}} \cdot \frac{d\mathbf{st}_{j+1}}{d\mathbf{dp}} \\ \frac{dE_{rj}}{d\mathbf{dp}} &= \frac{\partial E_{rj}}{\partial \mathbf{dp}} \\ \frac{\partial E_{rj}}{\partial \mathbf{m}_{j+1}} \text{ and } \frac{\partial E_{rj}}{\partial \mathbf{dp}} &\text{ is evaluated analytically and the } \frac{d\mathbf{m}_{j+1}}{d\mathbf{u}_i} \text{ is known analytically from the recurrence relation developed in Eqn. 6.} \end{aligned}$$

4) *Updating \mathbf{u} and \mathbf{dp}* : Let \mathbf{udp} be the optimization variable obtained after stacking \mathbf{u} and \mathbf{dp} . The gradients $\frac{d\mathcal{O}}{d\mathbf{u}}$ and $\frac{d\mathcal{O}}{d\mathbf{dp}}$ can be stacked to obtain the gradient $\frac{d\mathcal{O}}{d\mathbf{udp}}$. The optimization variable \mathbf{udp} in the current step of the trajectory optimization can be updated as follows:

$$\mathbf{udp}_{z+1} = \mathbf{udp}_z - \hat{\mathbf{H}}^{-1} \cdot \frac{d\mathcal{O}}{d\mathbf{udp}} \Big|_{\mathbf{udp}=\mathbf{udp}_z}$$

We approximate $\hat{\mathbf{H}}^{-1}$ using the L-BFGS quasi-Newton method. For standalone trajectory optimization only control inputs \mathbf{u} are optimized over a trajectory and design parameters \mathbf{dp} are kept fixed. For concurrent trajectory optimization both \mathbf{u} and \mathbf{dp} are optimized for prescribed objectives.

IV. SIMULATION RESULTS

A. Standalone trajectory optimization

We start with standalone trajectory optimization in which only control inputs \mathbf{u} are optimized over a trajectory and

design parameters \mathbf{dp} are kept fixed. In this subsection, we will discuss the core tasks \mathcal{O}_{task_i} in the objective function \mathcal{O} , in Eqn. 4. Please also refer to the accompanying video.

1) *Final end-effector state goal*: To demonstrate this task, we will use the 6-DOF simulation prototype shown in Fig. 1(b). This prototype has a combination of actuated joints, passive joints and mobile bases. The task, in the equation below, refers to the end-effector positioning of the CCMA system. $\mathbf{X}_{n_t-1}^*$ specifies the final end-effector pose, where as \mathbf{X}_{n_t-1} is the state of the CCMA system end-effector in the final state of the trajectory. \mathbf{X}_{n_t-1} is a function of \mathbf{st} .

$$\mathcal{O}_{task} = \mathcal{O}_{ee}(\mathbf{st}) = \frac{1}{2} \|\mathbf{X}_{n_t-1} - \mathbf{X}_{n_t-1}^*\|_2^2 \quad (7)$$

Fig. 3 shows the final trajectory obtained for the task of translating the end-effector by -3 m along \mathbf{x}_g , 3 m along \mathbf{y}_g and -0.5 m along \mathbf{z}_g with a rotation of about $+90$ deg about the \mathbf{z}_g . $n_t = 20$ states were used for this simulation. The input control vector was initialized with all zero values. Therefore, initial 20 CCMA states had the same values.

2) *Mobile agents internal collision avoidance*: While executing its tasks such as end-effector positioning, the CCMA system can have internal collision among the multiple mobile agents. In order to avoid this internal collision, we formulate a smooth continuously differentiable soft unilateral constraint $f_{pen}(x)$ which is defined below. Let lim be the minimum distance between the mobiles bases where an internal collision is just avoided. Let $dist_m$ be the actual distance between the mobile bases. Then $x = dist_m - lim$. For $x \leq 0$, a high value of $k = 10^4$ increases $f_{pen}(x)$ rapidly. For $0 < x \leq \epsilon$, where ϵ is a safety margin over lim , $f_{pen}(x)$ increases slowly. For $x > \epsilon$, $f_{pen}(x) = 0$.

$$\begin{aligned} f_{pen}(x) &= k \cdot \left(\frac{1}{2} \cdot x^2 - \frac{\epsilon}{2} \cdot x + \frac{\epsilon^2}{6} \right) & x \leq 0 \\ &= k \cdot \left(\frac{1}{6\epsilon} \cdot x^3 + \frac{1}{2} \cdot x^2 - \frac{\epsilon}{2} \cdot x + \frac{\epsilon^2}{6} \right) & 0 < x \leq \epsilon \\ &= 0 & x > \epsilon \end{aligned}$$

$dist_m(i, j, k)$ is the distance between mobile base pair (j, k) in the i^{th} state of the trajectory. This task and the corre-

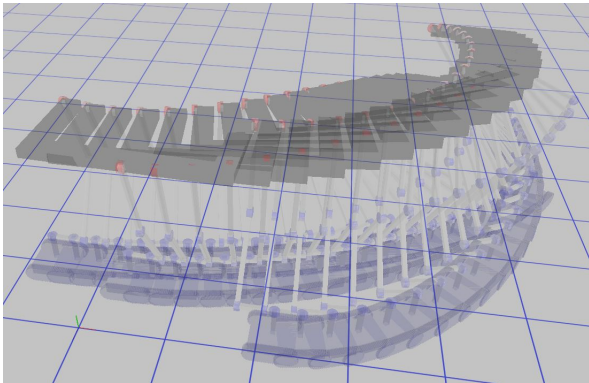


Fig. 3: A snapshot of 20 states in the trajectory for a translation plus rotation task of 6-DOF CCMA end-effector.

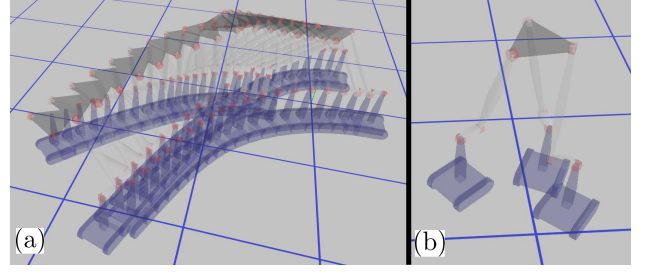


Fig. 4: Without the objective \mathcal{O}_{ica} (a) state trajectory for the end-effector positioning task (b) in the 10^{th} state of the trajectory, there is an internal collision between mobile bases.

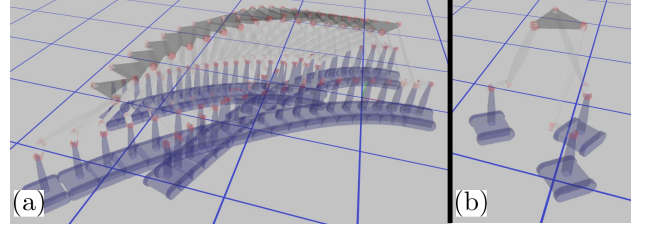


Fig. 5: With the objective \mathcal{O}_{ica} (a) state trajectory for the end-effector positioning task (b) in the 10^{th} state or any other state of the trajectory, there is no internal collision.

sponding objective function \mathcal{O}_{ica} is added to the Eqn. 4.

$$\mathcal{O}_{task} = \mathcal{O}_{ica}(\mathbf{m}) = \sum_{i=0}^{n_t-1} \sum_{j=0}^{n_m-1} \sum_{k=j+1}^{n_m-1} f_{pen}(dist_m(i, j, k))$$

The function $dist_m(i, j, k)$ is a function of \mathbf{m} and can be written as $dist_m(\mathbf{m})$.

To demonstrate this task, we will use a 4-DOF simulation prototype corresponding to Fig. 1(a) but with three kinematic chains and passive joints only. This prototype has no actuated joints. The Fig. 4 shows the trajectory plot obtained for the task of translating the end-effector by -2 m along \mathbf{x}_g , 2 m along \mathbf{y}_g with a rotation of about 90 deg about the \mathbf{z}_g . In the 10^{th} state, there is a collision between the mobile bases. Once the internal collision avoidance objective is added, the internal collision is avoided among the mobile bases, as can be seen in the Fig. 5.

3) *External obstacle avoidance*: We discretize each rigid body in the CCMA system into spheres of radius r with x, y, z co-ordinates of its center. In order to avoid static objects (considering cylindrical primitives, x, y co-ordinates and a radius), we formulate a soft unilateral constraint $f_{pen}(dist_o)$. $dist_o(i, j, k)$ is the distance between sphere j and the static object k in the i^{th} state of the trajectory. This task and the corresponding objective function \mathcal{O}_{eoa} is added to the Eqn. 4. n_{eo} is the number of static objects and n_s is the number of spheres in the discretized CCMA system.

$$\mathcal{O}_{task} = \mathcal{O}_{eoa}(\mathbf{m}, \mathbf{st}) = \sum_{i=0}^{n_t-1} \sum_{j=0}^{n_s-1} \sum_{k=0}^{n_{eo}-1} f_{pen}(dist_o(i, j, k))$$

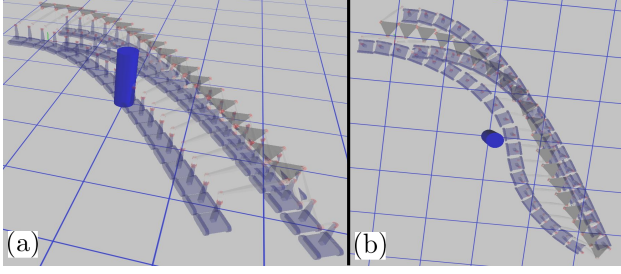


Fig. 6: (a) Without \mathcal{O}_{coa} , collision with a static object (b) with \mathcal{O}_{coa} , collision with a static object is avoided.

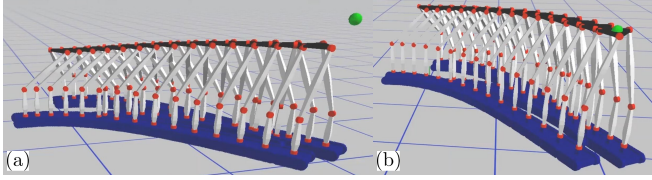


Fig. 7: (a) without and (b) with concurrent design and control policy evolution during trajectory optimization.

The function $\text{dist}_O(i, j, k)$ is a function of \mathbf{m} , \mathbf{st} and can be written as $\text{dist}_O(\mathbf{m}, \mathbf{st})$. As shown in Fig. 6, objective \mathcal{O}_{coa} helps avoid collision with the static object.

B. Concurrent control \mathbf{u} and design \mathbf{dp} optimization

\mathcal{O}_{ee} , \mathcal{O}_{coa} and Er_j are all functions of design parameters \mathbf{dp} as well. \mathcal{O}_{ee} task is a classical example of how the workspace of a system is affected by design parameters. In order to demonstrate concurrent optimization of control \mathbf{u} and design \mathbf{dp} parameters, we first obtain an initial trajectory for \mathcal{O}_{ee} task which is impossible to achieve with initial fixed design parameters. In second step, we do concurrent optimization but initialize the trajectory with previously calculated \mathbf{u} and initial design parameters. The final result is calculation of both optimal design and control parameters which concurrently evolve for satisfying the new workspace requirements, as demonstrated in Fig. 7. Please also refer to the full video¹.

V. EXPERIMENTAL RESULTS

In this section, we describe the experimental results which demonstrate the transfer of the simulation results for standalone trajectory optimization onto physical prototypes. Two fabricated physical prototypes are shown in the Fig. 8. For the end-effector motion shown in Fig. 9(a) & (b), the physical prototype in Fig. 8(a) & (b) were controlled to move 2 m along \mathbf{x}_g , 1 m along \mathbf{z}_g with a rotation of -90 deg about \mathbf{z}_g and 2 m along \mathbf{x}_g , 0.1 m along \mathbf{y}_g , 1 m along \mathbf{z}_g with a rotation of $+90$ deg about \mathbf{z}_g , respectively. The RMSE (Root Mean Square Error) were 0.038 m (along \mathbf{y}_g), 0.040 m (along \mathbf{z}_g), 0.072 m (along \mathbf{x}_g) and 0.062 rad (about \mathbf{z}_g) for plots in Fig. 9(a). RMSE (Root Mean Square Error) were 0.025 m (along \mathbf{y}_g), 0.038 m (along \mathbf{z}_g), 0.048 m (along

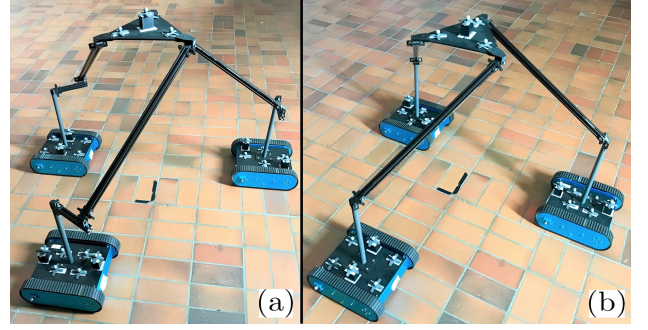


Fig. 8: The fabricated physical prototype in (a) corresponds to the simulated prototype in Fig. 4(b) which was also used for discussing different tasks $\mathcal{O}_{\text{task}}$ of the objective function \mathcal{O} in Sec. IV. The physical prototype in Fig. 8(b) has no offsets and it is a variant of the prototype in Fig. 8(a).

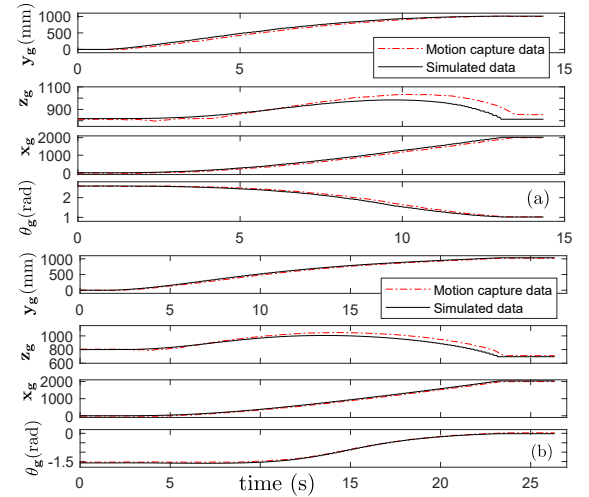


Fig. 9: Tracked and simulated motion of end-effector for prototype (a) in Fig. 8(a) (b) in Fig. 8(b) with a simultaneous translation along \mathbf{x}_g , \mathbf{y}_g , \mathbf{z}_g and rotation about \mathbf{z}_g .

\mathbf{x}_g) and 0.04 rad (about \mathbf{z}_g) for plots in Fig. 9(b). Please also refer to the accompanying video.

VI. DISCUSSION, CONCLUSIONS AND FUTURE WORK

We have developed a novel class of robotic systems having non-holonomic mobile bases, constrained by active-passive closed-loop kinematic chains manipulating an end-effector. We have also presented a novel trajectory optimization method which can handle concurrent optimization of both design and control parameters to solve different tasks from gross end-effector positioning, internal mobile agents collision avoidance to external obstacle collision avoidance.

In our future work, we would like to explore motion generation with heterogeneous combination of ground mobile robots ranging from omni-directional bases, mobile bases with non-holonomic constraints, quadruped robots and aerial mobile bases such as quadcopters. Going further, we will also explore the force transmission capabilities, concurrently with motion generation capabilities.

¹https://youtu.be/3ESmrf7_fXk

REFERENCES

- [1] R. Loveridge and T. Coray, "Robots on construction sites: The potential and challenges of on-site digital fabrication," *Science Robotics*, vol. 2, no. 5, p. eaan3674, Apr. 2017.
- [2] N. P. Hack, N. Kumar, J. Buchli, M. Kohler, and F. M. Gramazio, "Digital method and automated robotic setup for producing variable-density and arbitrary shaped metallic meshes," WO Patent WO2017153559A1, Sep., 2017.
- [3] N. Kumar, N. Hack, K. Doerfler, A. N. Walzer, G. J. Rey, F. Gramazio, M. D. Kohler, and J. Buchli, "Design, development and experimental assessment of a robotic end-effector for non-standard concrete applications," in *2017 IEEE International Conference on Robotics and Automation (ICRA)*, May 2017, pp. 1707–1713.
- [4] J. Buchli, M. Gifftthaler, N. Kumar, M. Lussi, T. Sandy, K. Dörfler, and N. Hack, "Digital in situ fabrication - Challenges and opportunities for robotic in situ fabrication in architecture, construction, and beyond," *Cement and Concrete Research*, vol. 112, pp. 66–75, Oct. 2018.
- [5] N. Hack, T. Wangler, J. Mata-Falcón, K. Dörfler, N. Kumar, A. Walzer, K. Graser, L. Reiter, H. Richner, J. Buchli, W. Kaufmann, R. Flatt, F. Gramazio, and M. Kohler, "MESH MOULD: AN ON SITE, ROBOTICALLY FABRICATED, FUNCTIONAL FORMWORK," in *Conference: High Performance concrete and Concrete Innovation Conference At: Tromsø, Norway Volume: 11th HPC and 2nd CIC*, Mar. 2017.
- [6] M. Gifftthaler, T. Sandy, K. Dörfler, I. Brooks, M. Buckingham, G. Rey, M. Kohler, F. Gramazio, and J. Buchli, "Mobile Robotic Fabrication at 1:1 scale: the In situ Fabricator," *Construction Robotics*, vol. 1, no. 1-4, pp. 3–14, Dec. 2017, arXiv: 1701.03573.
- [7] S. J. Keating, J. C. Leland, L. Cai, and N. Oxman, "Toward site-specific and self-sufficient robotic fabrication on architectural scales," *Science Robotics*, vol. 2, no. 5, p. eaam8986, Apr. 2017.
- [8] N. Kumar and S. Coros, "An optimization framework for simulation and kinematic control of Constrained Collaborative Mobile Agents (CCMA) system," in *2019 IEEE/RSJ International Conference on Intelligent Robots and Systems (IROS)*, Nov. 2019.
- [9] F. Augugliaro, S. Lupashin, M. Hamer, C. Male, M. Hehn, M. W. Mueller, J. S. Willmann, F. Gramazio, M. Kohler, and R. D'Andrea, "The Flight Assembled Architecture installation: Cooperative construction with flying machines," *IEEE Control Systems*, vol. 34, no. 4, pp. 46–64, Aug. 2014.
- [10] T. Rasheed, P. Long, D. Marquez-Gamez, and S. Caro, "Kinematic Modeling and Twist Feasibility of Mobile Cable-Driven Parallel Robots," in *Advances in Robot Kinematics 2018*, ser. Springer Proceedings in Advanced Robotics. Springer, Cham, Jul. 2018, pp. 410–418.
- [11] B. Zi, J. Lin, and S. Qian, "Localization, obstacle avoidance planning and control of a cooperative cable parallel robot for multiple mobile cranes," *Robotics and Computer-Integrated Manufacturing*, vol. 34, pp. 105–123, Aug. 2015.
- [12] Z. Wan, Y. Hu, J. Lin, and J. Zhang, "Design of the control system for a 6-DOF Mobile Parallel Robot with 3 subchains," in *2010 IEEE International Conference on Mechatronics and Automation*, Aug. 2010, pp. 446–451.
- [13] Y. Hu, Z. Wan, J. Yao, and J. Zhang, "Singularity and kinematics analysis for a class of PPUU mobile parallel robots," in *2009 IEEE International Conference on Robotics and Biomimetics (ROBIO)*, Dec. 2009, pp. 812–817.
- [14] Y. Hu, J. Zhang, Y. Chen, and J. Yao, "Type synthesis and kinematic analysis for a class of mobile parallel robots," in *2009 International Conference on Mechatronics and Automation*, Aug. 2009, pp. 3619–3624.
- [15] M. Gifftthaler, F. Farshidian, T. Sandy, L. Stadelmann, and J. Buchli, "Efficient kinematic planning for mobile manipulators with non-holonomic constraints using optimal control," in *2017 IEEE International Conference on Robotics and Automation (ICRA)*, May 2017, pp. 3411–3417.
- [16] P. R. Giordano, M. Fuchs, A. Albu-Schäffer, and G. Hirzinger, "On the kinematic modeling and control of a mobile platform equipped with steering wheels and movable legs," in *2009 IEEE International Conference on Robotics and Automation*, May 2009, pp. 4080–4087.
- [17] M. Geilinger, R. Poranne, R. Desai, B. Thomaszewski, and S. Coros, "Skaterbots: Optimization-based Design and Motion Synthesis for Robotic Creatures with Legs and Wheels," *ACM Trans. Graph.*, vol. 37, no. 4, pp. 160:1–160:12, Jul. 2018.
- [18] S. M. LaValle, "Planning Algorithms by Steven M. LaValle," May 2006.
- [19] J. P. Laumond, S. Sekhavat, and F. Lamiroux, "Guidelines in nonholonomic motion planning for mobile robots," in *Robot Motion Planning and Control*, ser. Lecture Notes in Control and Information Sciences, J. P. Laumond, Ed. Berlin, Heidelberg: Springer Berlin Heidelberg, 1998, pp. 1–53.
- [20] F. Jean, *Control of Nonholonomic Systems: from Sub-Riemannian Geometry to Motion Planning*, ser. SpringerBriefs in Mathematics. Springer International Publishing, 2014.
- [21] A. Dietrich, T. Wimböck, A. Albu-Schäffer, and G. Hirzinger, "Singularity avoidance for nonholonomic, omnidirectional wheeled mobile platforms with variable footprint," in *2011 IEEE International Conference on Robotics and Automation*, May 2011, pp. 6136–6142.
- [22] J. H. Yakey, S. M. LaValle, and L. E. Kavraki, "Randomized path planning for linkages with closed kinematic chains," *IEEE Transactions on Robotics and Automation*, vol. 17, no. 6, pp. 951–958, Dec. 2001.
- [23] T. McMahon, S. Thomas, and N. M. Amato, "Sampling-based motion planning with reachable volumes for high-degree-of-freedom manipulators," *The International Journal of Robotics Research*, vol. 37, no. 7, pp. 779–817, Jun. 2018.
- [24] G. Oriolo and C. Mongillo, "Motion Planning for Mobile Manipulators along Given End-effector Paths," in *Proceedings of the 2005 IEEE International Conference on Robotics and Automation*, Apr. 2005, pp. 2154–2160.
- [25] S. Coros, B. Thomaszewski, G. Noris, S. Sueda, M. Forberg, R. W. Sumner, W. Matusik, and B. Bickel, "Computational Design of Mechanical Characters," *ACM Trans. Graph.*, vol. 32, no. 4, pp. 83:1–83:12, Jul. 2013.
- [26] B. Thomaszewski, S. Coros, D. Gauge, V. Megaro, E. Grinspun, and M. Gross, "Computational Design of Linkage-based Characters," *ACM Trans. Graph.*, vol. 33, no. 4, pp. 64:1–64:9, Jul. 2014.
- [27] A. McNamara, A. Treuille, Z. Popović, and J. Stam, "Fluid Control Using the Adjoint Method," in *ACM SIGGRAPH 2004 Papers*, ser. SIGGRAPH '04. New York, NY, USA: ACM, 2004, pp. 449–456.
- [28] T. Auzinger, W. Heidrich, and B. Bickel, "Computational Design of Nanostructural Color for Additive Manufacturing," *ACM Trans. Graph.*, vol. 37, no. 4, pp. 159:1–159:16, Jul. 2018.
- [29] Y. Cao, S. Li, L. Petzold, and R. Serban, "Adjoint Sensitivity Analysis for Differential-Algebraic Equations: The Adjoint DAE System and Its Numerical Solution," *SIAM J. Sci. Comput.*, vol. 24, no. 3, pp. 1076–1089, Mar. 2002.
- [30] R. H. F. Jackson and G. P. McCormick, "Second-order sensitivity analysis in factorable programming: Theory and applications," *Mathematical Programming*, vol. 41, no. 1, pp. 1–27, May 1988.
- [31] S. Zimmermann, R. Poranne, J. M. Bern, and S. Coros, "PuppetMaster: Robotic Animation of Marionettes," *ACM Trans. Graph.*, vol. 38, no. 4, pp. 103:1–103:11, Jul. 2019.
- [32] J. Bern, P. Banzet, R. Poranne, and S. Coros, "Trajectory optimization for cable-driven soft robot locomotion," in *Proceedings of Robotics: Science and Systems*, Freiburg/Breisgau, Germany, June 2019.